JOURNAL OF GEOPHYSICAL RESEARCH, VOL. 115, A04101, doi:10.1029/2009JA014742, 2010

Click Here for Full Article

Magnetic energy distribution in the four-dimensional frequency and wave vector domain in the solar wind

Y. Narita,[1] F. Sahraoui,[2] M. L. Goldstein,[2] and K.-H. Glassmeier[1,3]

Received 7 August 2009; revised 26 October 2009; accepted 3 November 2009; published 1 April 2010.

[1] We present a measurement of the energy distribution in the four-dimensional (4-D) frequency and wave vector domain of magnetic field fluctuations in the solar wind. The measurement makes use of the wave telescope technique that has been developed particularly for multispacecraft data analysis. We review briefly the theoretical background and then present a numerical test using synthetic data; the technique is then applied to magnetic field data obtained while the Cluster spacecraft was in the solar wind. The energy distribution is determined in the flow rest frame in the frequency range below 0.2 rad/s and the wave number range below 0.0015 rad/km, corrected for the Doppler shift. We find the following properties in the energy distribution in the rest frame: (1) a double anisotropy in the wave vector domain associated with the mean magnetic field and the flow directions, (2) a symmetric distribution with respect to the sign of wave vector, and (3) no evidence for a linear dispersion relation in the frequency and wave number domain. Since the flow direction in the analyzed time interval is close to the normal direction to the bow shock, the anisotropy may well be associated with the bow shock. These results suggest that the solar wind is in a state of well-developed strong turbulence and justifies the theoretical picture of quasi-two-dimensional turbulence that obtains in the presence of a (relatively) strong DC magnetic field. However, the fluctuations are not axisymmetric around the mean field and the energy distribution is extended in the perpendicular direction to the flow or shock normal. Anisotropy associated with the boundary is reminiscent of previously reported magnetosheath turbulence. This study opens a way to investigate solar wind turbulence in the full 4-D frequency and wave vector space.

Citation: Narita, Y., F. Sahraoui, M. L. Goldstein, and K.-H. Glassmeier (2010), Magnetic energy distribution in the four-dimensional frequency and wave vector domain in the solar wind, *J. Geophys. Res.*, *115*, A04101, doi:10.1029/2009JA014742.

1. Introduction

[2] Magnetic field fluctuations in the solar wind are believed to be in a fully developed turbulent state and thus the solar wind serves as a natural laboratory for studying turbulence in collisionless magnetofluids. Early spacecraft observations revealed that frequency spectra of solar wind magnetic field fluctuations showed an inertial-like range that resembled Kolmogorov turbulence in fluids [*Coleman*, 1968; *Kolmogorov*, 1941]. Indeed, Coleman's early work and subsequent investigations have demonstrated that the spectral index in the inertial range is commonly very close to −5/3 [*Matthaeus and Goldstein*, 1982; *Matthaeus et al.*, 1982; *Marsch and Tu*, 1990; *Leamon et al.*, 1998; *Podesta et al.*, 2007], which is the index Kolmogorov derived from general principles for isotropic, incompressible, hydrodynamic turbulence. Of course, the solar wind is not a Navier-Stokes fluid, nor are the magnetic fluctuations isotropic. Furthermore, the fluid fluctuations are not incompressible. Trying to understand why the magnetic fluctuations in the solar wind so closely resemble those of a simple Navier-Stokes fluid has been an area of intense interest for more than 40 years.

[3] Using Taylor's hypothesis and projecting magnetic field fluctuations to the axis parallel and perpendicular to the mean magnetic field, *Matthaeus et al.* [1990] found that the fluctuations were anisotropic and appeared to consist of a population of planar fluctuations with large correlations perpendicular to the mean magnetic field and a second population with large correlations parallel to the mean magnetic field. In other words, the solar wind fluctuations consisted of two components: a planar (slab) component and a two-dimensional component. Owing to a paucity of data, *Matthaeus et al.* [1990] had to assume that the fluctuations were axisymmetric about the background DC magnetic field. Subsequent work [e.g., *Dasso et al.*, 2005] also confirmed this anisotropy but also noted that fast and slow solar wind seemed to be dominated by one or the other component.

[4] Previously, studies of the spectra of magnetic field fluctuations have been based on single point measurements. Frequency spectrum should be a reasonable reflection of

[1]Institut für Geophysik und extraterrestrische Physik, Technische Universität Braunschweig, Braunschweig, Germany.
[2]Geospace Physics Laboratory, NASA Goddard Space Flight Center, Greenbelt, Maryland, USA.
[3]Max-Planck-Institut für Sonnensystemforschung, Katlenburg-Lindau, Germany.

Copyright 2010 by the American Geophysical Union.
0148-0227/10/2009JA014742

wave number spectra in the flow direction because Taylor's frozen-in flow hypothesis [*Taylor*, 1938] is well justified in the supersonic, super-Alfvénic solar wind. Under this hypothesis, temporal variations are interpreted as spatial variations in the flow direction and one obtains a reduced one-dimensional spectrum that is averaged over direction perpendicular to the flow. To determine the 3-D structure of the power spectral tensor at a single time requires multipoint measurements (recall that the results of *Matthaeus et al.* [1990] depended on the assumption that the ergodic theorem was valid, namely, that all the samples analyzed belonged to the same statistical ensemble).

[5] In this paper we address a fundamental question that we hope will advance our understanding of solar wind turbulence, namely, what is the 3-D structure of the power spectral density of magnetic fluctuations in the solar wind? To accomplish this requires an analysis of the full four-dimensional (4-D) frequency and wave number energy distribution of the magnetic fluctuations. Below, we determine the energy distribution in both the spacecraft and flow rest frames (which requires a Doppler shift correction).

[6] Cluster magnetometer data [*Balogh et al.*, 2001; *Escoubet et al.*, 2001] is ideal for studying waves and turbulence in the solar wind and nearby regions upstream and downstream of Earth's bow shock. Measuring fields and/or particles at four points in space enables one to distinguish between temporal and spatial variations and makes it possible to determine spatial structures in space. There are a variety of analysis tools that have been developed specifically for multipoint missions; these include tools to perform dispersion analyses [*Narita et al.*, 2003, 2007; *Narita and Glassmeier*, 2005; *Sahraoui et al.*, 2003; *Tjulin et al.*, 2005; *Vogt et al.*, 2008], to discern propagation patterns [*Narita et al.*, 2004; *Narita and Glassmeier*, 2006; *Narita et al.*, 2006a], and to determine energy spectra in the wave number domain [*Narita et al.*, 2006b, 2007; *Sahraoui et al.*, 2004, 2006]. For a recent review of multipoint turbulence analysis methods, see *Horbury and Osman* [2008]. *Sahraoui et al.* [2010] have studied various technical aspects and limitations of the wave telescope technique (or *k*-filtering technique) when applied to Cluster data by providing (1) an accurate estimation of the resolution of the wave number domain, (2) boundary conditions in the (ω, $\mathbf{k}$) space necessary to perform a proper integration of the energy distribution and to obtain reduced wave number spectra, (3) a description of the aliasing problem and the role of the Doppler shift in the symmetry breaking (ω_{rest}, $\mathbf{k}$) $\rightarrow$ ($-\omega_{rest}$, $-\mathbf{k}$) (the subscript "rest" indicates measurement in the flow rest frame), and (4) an explanation of artificial anisotropies of the wave number spectra of turbulence that occur if a nonregular tetrahedron of the spacecraft is used. These limits are considered in the present work and our results confirm some of the predictions given by *Sahraoui et al.* [2010].

[7] The organization of this paper is as follows: Section 2 contains a brief description of the wave telescope technique. This is followed in section 3 by a numerical test using synthetic data. Section 4 contains application to Cluster observations of magnetic field fluctuations in the solar wind. The results are interpreted in section 5, and conclusions are given in section 6.

2. Estimating 4-D Energy Distributions Using the Wave Telescope Method

[8] Ideally, one would like to have as many properly spaced spacecraft available as possible to Fourier transform observed fluctuations from the spatial coordinates into wave numbers. The four Cluster spacecraft are too few for performing the Fourier transform into a broad wave number domain, but it is possible to estimate the energy distribution in the 4-D frequency and wave vector domain using only four points with the methods known as either "wave telescope" or "*k*-filtering" [*Pinçon and Lefeuvre*, 1988, 1991; *Neubauer and Glassmeier*, 1990; *Motschmann et al.*, 1996; *Glassmeier et al.*, 2001]. For magnetic field fluctuations measured by Cluster, these techniques make use of the full 12 × 12 cross-spectral density matrix (correlation matrix) of the measurements (three components of the magnetic field by four spacecraft) to estimate the 4-D spectral energy density denoted here by $P(\omega, \mathbf{k})$. These methods do not assume any physics about the data under study, such as an existing linear dispersion relation or the weak (or strong) nature of nonlinearities. In this sense, the methods are the most generally applicable to space plasma turbulence. These methods allow one, furthermore, to include further theoretical constraints that might be appropriate, such as the divergence-free equation for magnetic field fluctuations, namely, $\nabla \cdot \delta\mathbf{B} = 0$.

3. Numerical Test

[9] Although the wave telescope has been successfully applied to determine the first 3-D *k*-spectra of low-frequency magnetosheath turbulence [*Sahraoui et al.*, 2006], we show here a similar application to synthetic data to test the robustness of the technique in reconstructing a known 3-D energy distribution. For this purpose, we generate numerically random fluctuating magnetic field using a model energy distribution and sample the fluctuations as time series data at four distinct sensors in a regular tetrahedron formation. As shown by *Sahraoui et al.* [2010], it is essential that the four sensors form a regular tetrahedron in order to apply the wave telescope technique to avoid the appearance of artificial energy anisotropies and spatial aliasing that distorts the measured energy distribution [*Pinçon and Motschmann*, 1998; *Sahraoui et al.*, 2003; *Narita and Glassmeier*, 2009]. Here we apply the wave telescope technique to these time series and reconstruct the energy distribution. In the numerical test the data are considered in the flow rest frame (i.e., the stationary frame). Therefore the fluctuations propagate past the satellites with phase speeds given by $V_\phi = \omega_0/|\mathbf{k_0}|$, where ω_0 and $\mathbf{k_0}$ are the angular frequency and the wave vector of the chosen wave plane, respectively.

3.1. Model Distribution

[10] We assume an isotropic power law energy distribution in both frequency and wave vector domains,

$$E_{model}(f, \mathbf{k}) \propto \left(\sqrt{\left(\frac{f}{f_0}\right)^2 + \left(\frac{|\mathbf{k}|}{k_0}\right)^2} \right)^{\alpha}, \qquad (1)$$

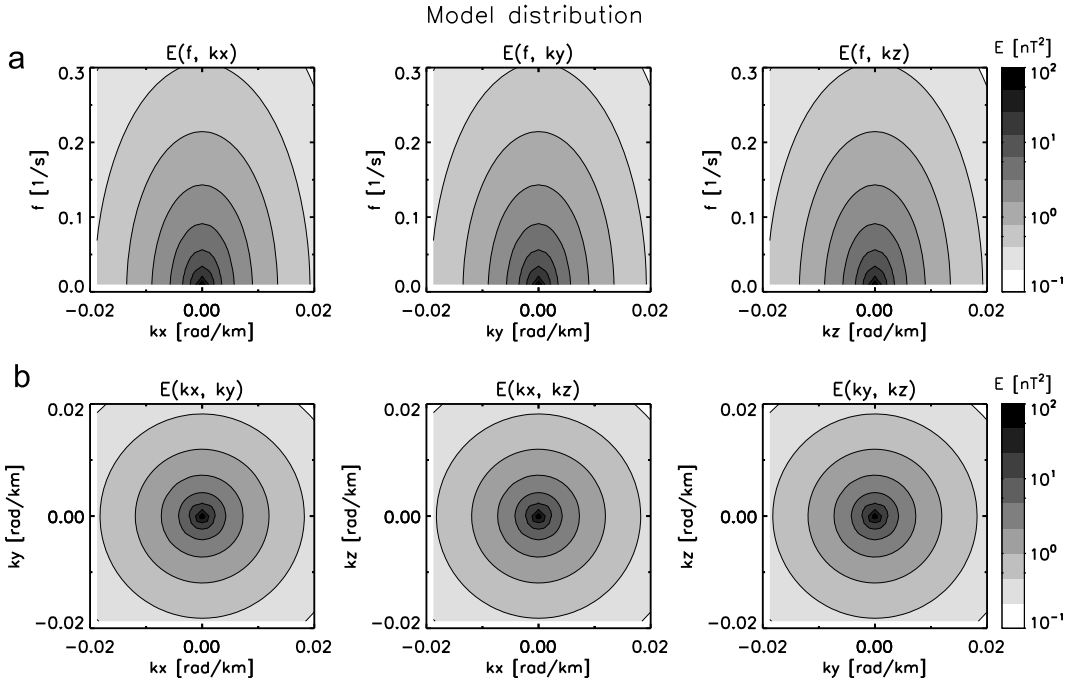

Figure 1. Model energy distribution model used for the numerical test, showing (a) projection (summing over frequencies and averaging over wave numbers) of the distribution into the planes spanned by frequency and wave numbers and (b) projection into the planes spanned by wave number and the other wave numbers.

where $\alpha = -11/3$. The value of the index $-11/3$ is associated with the 3-D Komogorov scaling [*Biskamp*, 2003], f_0 and k_0 are reference frequency and wave number, and we use the values of $f_0 = 0.3$ Hz and $k_0 = 0.02$ rad/km. Other choices of the model distribution such as a Gaussian distribution are also possible, but here we use a distribution that exhibits a power law in the 4-D frequency and wave number domain. Figure 1 displays projections of the model 4-D distribution into six different planes: three of them are spanned by the frequency and the wave numbers (f-k_x, f-k_y, and f-k_z planes, shown in Figure 1a) and the other three planes are spanned by the wave numbers ($k_x - k_y$, $k_x - k_z$, and $k_y - k_z$ planes, shown in Figure 1b). Here, by "projection" of the 4-D distribution, we mean a summation over frequencies together with an averaging over wave numbers.

[11] Magnetic field fluctuations are numerically generated based on the model distribution above. Frequencies and wave vectors of 400 mutually incoherent plane waves, with random initial phases, are randomly drawn from a uniform distribution in this 4-D parameter space. Wave amplitudes are determined by the square root of the energy distribution at various sets of frequency and wave vector. Wavefields are transverse to the wave vector direction to satisfy the divergence-free nature of magnetic field. These wavefields are superposed on a constant mean magnetic field, 10 nT in all the B_x, B_y, B_z components. We sample the generated magnetic field fluctuation at four distinct points forming a regular tetrahedron with the separation 100 km.

[12] The coordinate system in the numerical test is spanned by the reciprocal vectors of the tetrahedron, in which (1) the origin is the center of tetrahedron, (2) the z axis is parallel to the reciprocal vector $\mathbf{k}_a$ (in the direction from the plane of sensor 1, 2, and 3 to sensor 4), and (3) the xz plane is spanned by two vectors $\mathbf{k}_a$ and $\mathbf{k}_b$ (in the direction from the plane sensor 1, 3, and 4 to sensor 2). The sensor positions in the spatial coordinate are $\mathbf{r}_1$ = (−38.49, 66.67, −27.22) km, $\mathbf{r}_2$ = (48.11, 16.67, −27.22) km, $\mathbf{r}_3$ = (−38.49, −33.33, −27.22) km, $\mathbf{r}_4$ = (−9.62, 16.67, 54.43) km, respectively. The reciprocal vectors $\mathbf{k}_a$, $\mathbf{k}_b$, and $\mathbf{k}_c$ are associated with the position vectors and obtained as follows [*Neubauer and Glassmeier*, 1990]:

$$\mathbf{k}_a = \mathbf{k}_{123} = 2\pi \frac{\mathbf{r}_{12} \times \mathbf{r}_{13}}{\mathbf{r}_{14} \cdot (\mathbf{r}_{12} \times \mathbf{r}_{13})} \tag{2}$$

$$\mathbf{k}_b = \mathbf{k}_{134} = 2\pi \frac{\mathbf{r}_{13} \times \mathbf{r}_{14}}{\mathbf{r}_{12} \cdot (\mathbf{r}_{13} \times \mathbf{r}_{14})} \tag{3}$$

$$\mathbf{k}_c = \mathbf{k}_{142} = 2\pi \frac{\mathbf{r}_{14} \times \mathbf{r}_{12}}{\mathbf{r}_{13} \cdot (\mathbf{r}_{14} \times \mathbf{r}_{12})}. \tag{4}$$

The fourth reciprocal vector is a combination of the other three vectors, $\mathbf{k}_d = -\mathbf{k}_a - \mathbf{k}_b - \mathbf{k}_c$. In the numerical test these vectors are specifically expressed as $\mathbf{k}_a$ = (0.000, 0.000, 0.077) rad/km, $\mathbf{k}_b$ = (0.073, 0.000, −0.026) rad/km, $\mathbf{k}_c$ = (−0.036, −0.063, −0.026) rad/km, $\mathbf{k}_d$ = (−0.036, 0.063, −0.026) rad/km. The configuration of tetrahedron is conveniently given by the tetrahedron geometry factor, Q_{GM} [*Robert et al.*, 1998]. It is defined as

$$Q_{GM} = \frac{V}{V_{id}} + \frac{S}{S_{id}} + 1, \tag{5}$$

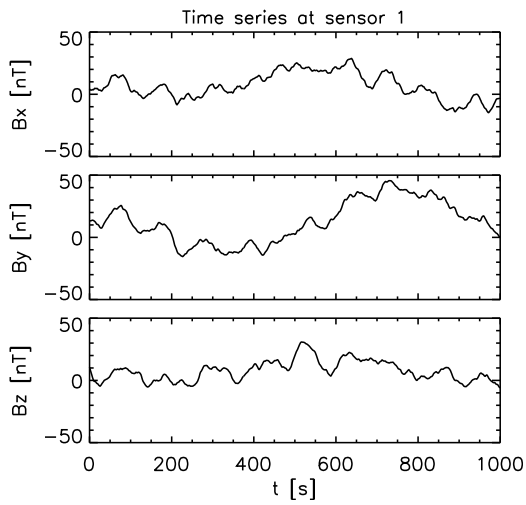

Figure 2. Time series of the synthetic magnetic field data at sensor 1.

where V and S are the volume and the surface area of the tetrahedron, and they are compared to that of an ideal, regular tetrahedron, V_{id} and S_{id}, respectively. The value $Q_{GM} = 1$ means that the sensors are in one-dimensional array, the value $Q_{GM} = 2$ means that the four sensors are in a plane, and the value $Q_{GM} = 3$ means that they form a regular tetrahedron.

[13] The synthetic magnetic field data are displayed in Figures 2 and 3. The former is time series data sampled at the sensor 1, and the latter is spatial variation of magnetic field at the initial time $t = 0$. The spatial variation is sampled separately from the time variation. Both the temporal and the spatial data show an irregular pattern of magnetic field, reflecting random phases of waves.

3.2. Reconstructed Distribution

[14] The wave telescope technique is applied to the synthetic magnetic field data generated above. The energy distribution is determined in the frequency range $f < 0.3$ Hz and the wave vector range $|\mathbf{k}| < 0.02$ rad/km. Figure 4 displays six-plane projections of the obtained 4-D energy distribution. Dotted lines indicate the directions of reciprocal vectors. All four reciprocal vectors are plotted in Figure 4b, but the fourth vector is not clearly visible because we chose a coordinate system that is determined by the set of the reciprocal vectors itself. In the xy plane the fourth reciprocal vector is in the direction out of the plane (z-component only). In the xz plane two of the four vectors degenerate (the line from bottom left to top right). One is in the direction out of the plane and the other is toward the plane. In the yz plane two of the vectors again degenerate along the k_z axis. One is pointed to a positive k_z and the other is to a negative k_z.

[15] The first thing to note is that the overall shape of the energy distribution in the projection plots in the frequency and the wave vector more or less reflect the model distribution. The reconstructed distribution exhibits maximum at lowest frequencies and smallest wave vectors both in the frequency and in the wave vector, and energy decreases toward higher frequencies and larger wave vectors monotonously. The energy distribution in the 3-D wave vector domain (Figure 4b) is isotropic overall but is accompanied by slight distortions more visible at small wave vectors. This effect has been also observed by *Sahraoui et al.* [2010] and explained as arising from uncertainties in estimating spatial scales much larger than the spacecraft separations. Another effect is degeneracy of spatial sampling points in the reciprocal vector directions. The tetrahedron configuration of the sensors are projected to four different points in various one-dimensional cuts, but the four points degenerate into only two points when projected into the directions of the reciprocal vectors. For example, the vector $\mathbf{k}_a = \mathbf{k}_{123}$ is in the direction normal to the plane spanned by the three sensors $\mathbf{r}_1$, $\mathbf{r}_2$, and $\mathbf{r}_3$, and the last sensor $\mathbf{r}_4$ is out of this plane. For a plane wave in the this direction we have only two points because the three points $\mathbf{r}_1$, $\mathbf{r}_2$, and $\mathbf{r}_3$ are projected to the same position in this projection. This means that we have only two points to measure a wave phase difference in the reciprocal vector directions and that results in overestimate or underestimate of the energy. The difference of the energy distribution between the maximum and the minimum energy directions is about 33% from their mean values in the $k_x - k_y$ plane, i.e., 33% fluctuation in the energy distribution is due to the measurement effects. In the $k_x - k_z$ plane the difference is smaller and the fluctuation is about 29% from the mean values. In the $k_y - k_z$ plane it is even smaller, 6%. Therefore maximum about 33% uncertainty in the energy distribution should be taken into account for the anisotropy study even though we use a regular tetrahedron configuration for the sensor array.

[16] In the frequency domain the wave telescope technique uses the Fourier transform and the energy estimate is accurate. We use a small frequency interval $\Delta f = 0.0039$ Hz in the numerical test and the frequency resolution is about 1.3% of the plotted frequency range. In the wave vector direction the technique uses a projection method with a resolution $\Delta k = 0.0005$ rad/km, or a relative resolution of 2.5%. This resolution is the maximum we can use here as estimated by *Sahraoui et al.* [2010], since smaller Δk, or equivalently larger scales, are subject to error bars of 100%. This lack of resolution in the k-space as compared with the frequency domain may explain the broadening of the energy distribution in the wave number domain. We also note that

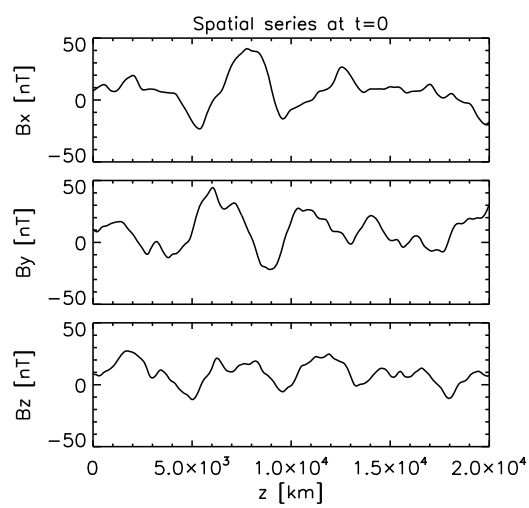

Figure 3. Spatial series of the synthetic magnetic field data at the initial time.

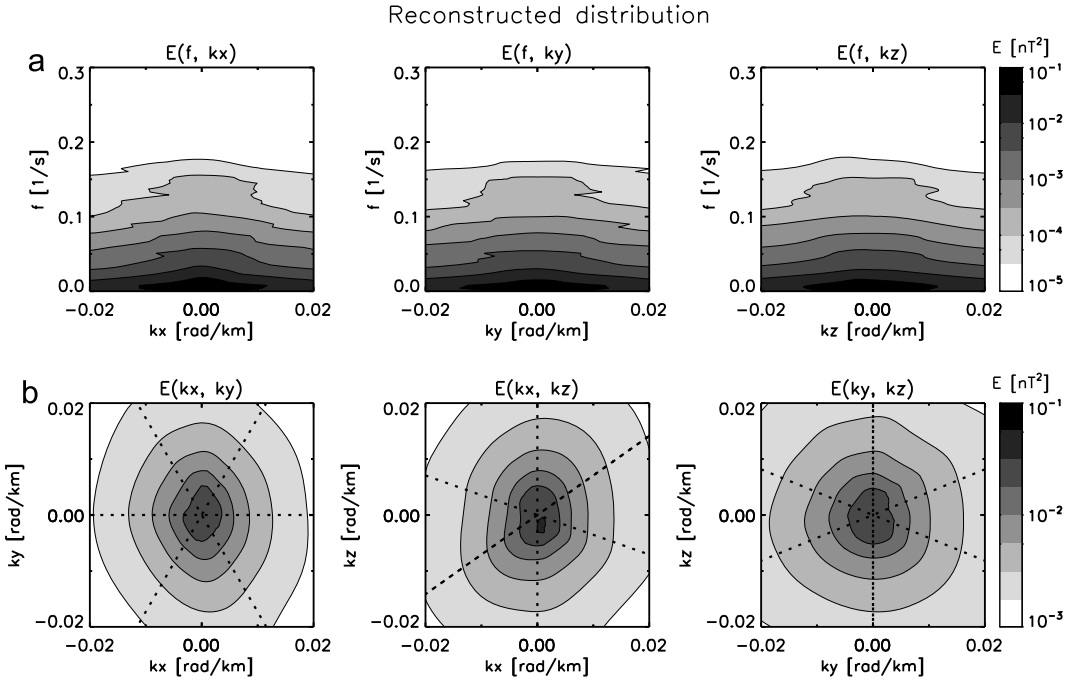

Figure 4. Energy distribution reconstructed from the synthetic magnetic field data at four points. The projection style is the same as Figure 1. Dotted lines in Figure 4b indicate directions of the reciprocal vectors of the tetrahedron sensor configuration.

the wave telescope technique requires an exact matching between the true wave vector and the analyzed wave vector and a mismatch between them results in slightly different estimates of the energy.

[17] We conclude this section by addressing that it is indeed possible to determine the 4-D energy distribution based on four-point measurements only and that the overall shape of the distribution reflects the true distribution. Slight distortions of the distribution can affect large scales due to large uncertainties *Sahraoui et al.* [2010].

4. Cluster Observations in the Solar Wind

[18] Here we apply the wave telescope technique to magnetic field fluctuations in the solar wind to determine the 4-D energy distribution in the flow rest frame. This requires us to first to determine the distribution in the spacecraft frame and then to use the supersonic and super-Alfvénic flow speeds of the solar wind to Doppler shift the frequencies into the plasma flow frame of reference.

[19] We use the Cluster observations of 12 March 2005, from 1800 to 2200 UT. Figure 5 displays the magnetic field data obtained by fluxgate magnetometer (FGM) instrument on board Cluster-1 [*Balogh et al.*, 2001]. The mean magnetic field is slowly rotating but on average it is $\mathbf{B}_0 = (-0.52, -1.60, 0.94)$ nT in the GSE coordinate system with the strength 1.85 nT. The mean flow velocity is about $\mathbf{V} = (-362, 32, 14)$ km/s in GSE and the average density is about $n = 4\ \mathrm{cm}^{-3}$, as measured by the CIS-HIA instrument (the ion electrostatic analyzer) [*Rème et al.*, 2001]. The flow velocity and the mean magnetic field form an angle of 75°. We chose this time interval because Cluster was close to apogee in its polar orbit and was almost stationary in the solar wind at 17 R_E ahead of the Earth (1 R_E = 6371 km). More importantly, the tetrahedral configuration of Cluster was almost regular (Q_{GM} varied from to 2.96 to 2.77 during this time interval). This is a requirement necessary to ensure the proper determination of the 3-D wave vector spectra [*Sahraoui et al.*, 2010]. The interspacecraft distance was about 1000 km (minimum separation 800 km and maximum separation 1200 km).

[20] In the analysis we use a flow coordinate system in which the z-axis is parallel to the flow direction and the xz plane is spanned by the flow direction and the mean

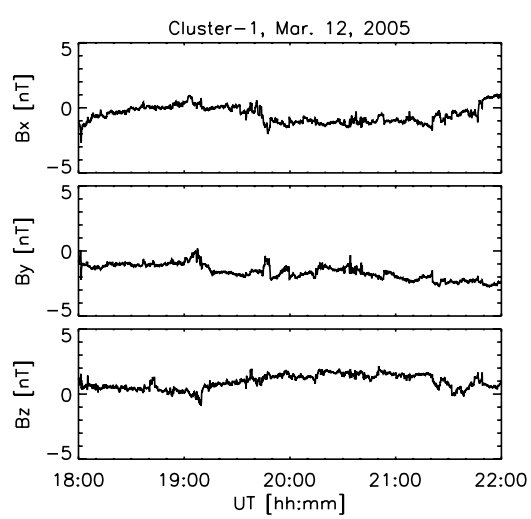

Figure 5. Time series of the solar wind magnetic field as measured by Cluster 1 in GSE coordinates.

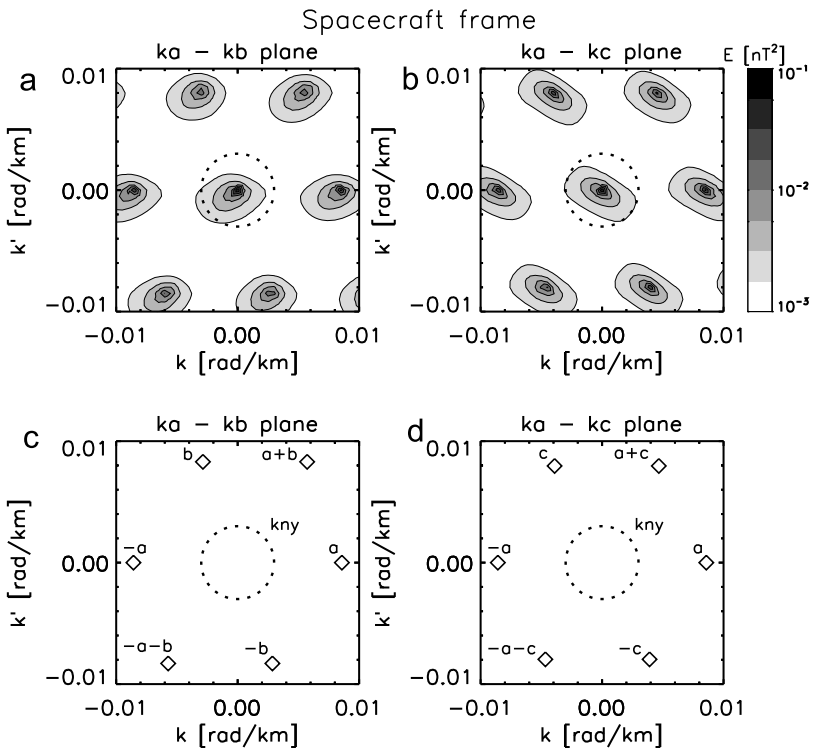

Figure 6. Projection of energy distribution into planes (a) spanned by the reciprocal vectors $\mathbf{k}_a$ and $\mathbf{k}_b$ and (b) spanned by $\mathbf{k}_a$ and $\mathbf{k}_c$. Also shown are (c and d) lattice points spanned by these vectors, where the letters a, b, and c denote the reciprocal vectors. Dotted circles are the Nyquist wave number (k_{ny}) used in the analysis.

magnetic field. In this coordinate system the mean magnetic field is $\mathbf{B}$ = (1.80, 0.00,0.41) nT, the flow velocity $\mathbf{V}$ = (0.00, 0.00,364) km/s, and the reciprocal vectors are $\mathbf{k}_a = \mathbf{k}_{123}$ = (−0.00317, 0.00768, −0.00211) rad/km, $\mathbf{k}_b = \mathbf{k}_{134}$ = (0.00861, −0.00010, −0.00169) rad/km, $\mathbf{k}_c = \mathbf{k}_{142}$ = (−0.00482, −0.00703, −0.00245) rad/km. We split the time interval into 100 windows each with an interval of 256 s. In each time window the flow direction and the mean magnetic field direction are determined to establish the flow coordinate system. The Fourier transform is applied to obtain frequency spectra of magnetic field fluctuations at each spacecraft. The frequency spectra are then averaged over the split time windows and the wave telescope technique is applied to the averaged frequency spectra.

[21] The procedure used is as follows.

[22] 1. We determine the 4-D energy distribution in the spacecraft frame and examine its properties and discuss briefly the aliasing problem (section 4.1).

[23] 2. We transform the obtained 4-D energy distribution into the flow rest frame by correcting from the Doppler shift. We investigate the resulting asymmetries in the (ω_{rest}, $\mathbf{k}$) domain (section 4.2).

[24] 3. We integrate over ω_{rest} to obtain the 3-D k-spectra and investigate the resulting anisotropies (section 4.3).

4.1. Four-Dimensional Distribution in the Spacecraft Frame

[25] One of the fundamental assumptions used in the wave telescope technique is that all wavelengths in the data are larger than the average spacecraft separation. This allows one to define the wave number domain of the analysis by the reciprocal vectors, which for this interval, yields the Nyquist wave number $k_{\max} \sim 0.003$ rad/km. Therefore all the spatial scales within the data are assumed to belong to the domain $[-k_{\max}, k_{\max}]$. If smaller scales exist, then spatial aliasing will occur. This limit is indicated in Figure 6 with a dotted circle. In the work of *Sahraoui et al.* [2010] it has been shown that the smallest wave number that we can determine accurately is $k_{\min} \sim k_{\max}/50$, which yields here $k_{\min} \sim 6 \times 10^{-4}$ rad/km. It has been also shown by the same authors that in order to limit, or idealistically to suppress, the spatial aliasing effect one needs to restrict the analysis to a maximum frequency in the spacecraft frame given roughly by $f_{\max} \sim k_{\max}(V_f + V_\phi)$, where V_f is the flow speed and V_ϕ is a given phase speed of the medium. Here since $V_\phi \ll V_f$, we obtain $f_{\max} \sim k_{\max} V_f/2\pi \sim 0.14$ Hz (Figure 7). Consequently, our analysis is limited to the domain $f_{sc} < 0.14$ Hz and $|k| < 0.003$ rad/km as shown in Figure 8.

[26] Figures 6a and 6b display two examples of the energy distribution in the spacecraft frame. The distribution is projected (summed over frequencies and averaged over wave numbers) into two planes that are spanned by the reciprocal vectors. Projection into the first and the second reciprocal vectors ($\mathbf{k}_a$ and $\mathbf{k}_b$) is displayed in Figure 6a. The energy distribution around the origin $\mathbf{k}$ = (0, 0) rad/km (we call it the principal distribution) appears repeatedly, and the periodic structure agrees with the lattice points spanned by the reciprocal vectors. Figure 6c shows the two reciprocal vectors $\mathbf{k}_a$ and $\mathbf{k}_b$ for comparison. We can see that aliases of the principal distribution appear at all linear combinations of

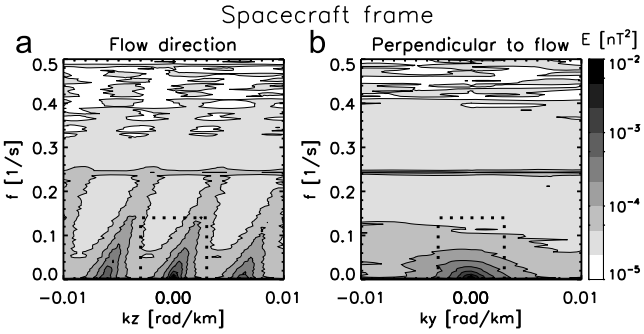

Figure 7. Aliases in the frequency and wave vector domain.

the reciprocal vectors (e.g., $\mathbf{k}_a + \mathbf{k}_b$ and $-\mathbf{k}_a - \mathbf{k}_b$). Spatial aliasing under the Cluster observation is also discussed by several authors [*Pinçon and Lefeuvre*, 1988; *Glassmeier et al.*, 2001; *Sahraoui et al.*, 2003; *Tjulin et al.*, 2005; *Narita and Glassmeier*, 2009].

[27] Figure 7 displays two cuts of the energy distribution in the plane of spacecraft frame frequency f and wave number in the flow direction (f-k_z plane, Figure 7a) and in the plane of the frequency and wave number perpendicular to the flow (f-k_y plane, Figure 7b). In the f-k_z plane the principal distribution has an extended structure from low frequencies and smaller wave numbers to higher frequencies and positive wave numbers (from the origin to the right top direction in the plot). Its apparent phase speed agrees roughly with the flow speed $2\pi f_{sc}/k_z$ = 393 km/s, suggesting that this dispersion relation in the energy distribution is predominantly due to the flow effect. The energy distribution exhibits in addition an enhanced line at the spacecraft frame spin frequency, 0.25 Hz (4 s spin). The principal distribution appears periodically both at the positive and negative wave numbers in the f-k_z plane. They are aliases of the principal distribution with the interval of aliasing wave number k = 0.006 rad/km, which limited our range in the previous wave vector analysis. It is important to note that the aliases of the principal distribution crosses the Nyquist wave number at higher frequencies and the periodic pattern is identified in the energy distribution not only in the wave number domain but also in the frequency domain with the interval about k = 0.006 rad/km and f = 0.35 Hz, respectively. This is the spatiotemporal aliasing and it originates in the apparent dispersion relation in the energy distribution (imposed by the flow in this case), and the interval of frequency aliases is determined by the apparent phase speed and the aliasing wave number. This shows clearly the necessity to restrict the analyzed frequency domain to $f_{\max}$ = 0.14 Hz to avoid the apparent aliases. Note that although the fluxgate magnetometer performs a high-sampling rate 22 Hz, we are limited to a small frequency range, even smaller than that of spacecraft spin (0.25 Hz). The range of the frequency and the wave number (f_{sc} < 0.14 Hz and k_z < 0.003 rad/km) is indicated as a dotted square in Figure 7. In this range the energy distribution is assumed to be dominated by the principal distribution, not by its aliases. In the f-k_y plane there is no flow effect or dispersion relation in the energy distribution (Figure 7b). Furthermore the aliasing wave number is larger than 0.01 rad/km and no periodic pattern is identified in Figure 7. We use, however, the same frequency and wave number range as determined for the energy distribution in the flow direction. The range is indicated with a dotted square as well (Figure 7b).

[28] The 4-D energy distribution in the spacecraft frame is displayed in Figure 8 as projections into the three planes of frequency and wave number f-k_x, f-k_y, and f-k_z, by averaging over the other two wave number directions. In the flow direction (the f-k_z plane, Figure 8a) the distribution exhibits an extended structure from (f, k_z) = (0.00 Hz, 0.000 rad/km) to (0.14, Hz, 0.025 rad/km) and the slope $2\pi f/k_z$ agrees roughly with the flow speed. Most of fluctuation energy is found in the direction parallel to the flow with a little energy antiparallel to the flow, which reflects the fact that the solar wind is supersonic and super-Alfvénic and most of the fluctuations are simply being convected past the spacecraft. Projections of the energy distributions perpendicular to the flow (the f-k_x and the f-k_y planes) are more symmetric between the positive and the negative wave numbers and show no clear dispersion relation.

[29] A 95% confidence interval is estimated for the projected energy distributions. It is displayed as a small vertical bar at the energy scale bar in Figure 8. The confidence interval is determined by the number of degrees of freedom used for the statistical average in the analysis, assuming that the estimate of energy follows a normal distribution [*Jenkins and Watts*, 1968]. We use 1200 degrees of freedom for averaging (100 time windows, three component of magnetic field, and four spacecraft). The confidence interval is smaller

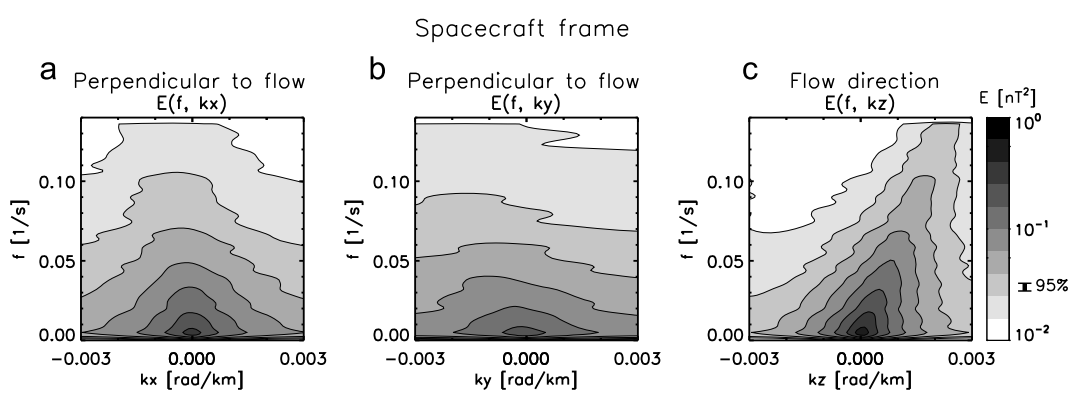

Figure 8. Energy distribution in the spacecraft frame determined from Cluster data obtained on 12 March 2005.

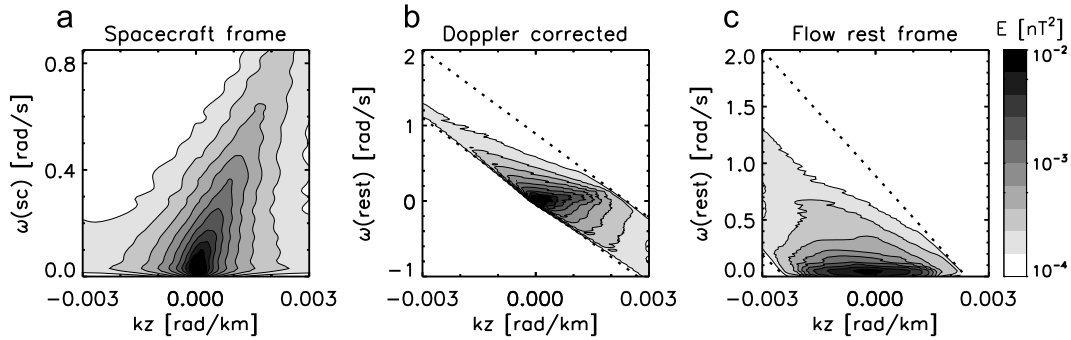

Figure 9. Cuts of energy distribution in the frequency and the wave number plane in the direction of the flow. The frequencies are (a) in the spacecraft frame, (b) in the flow rest frame obtained by the Doppler shift correction, and (c) in the flow rest frame with absolute frequency representation.

than the step of energy scale contours; therefore statistical error in the determined energy distribution is not significant.

4.2. Doppler Shift Correction

[30] To obtain the energy distribution in the flow rest frame, we correct for the Doppler shift using the relation,

$$\omega_{rest} = \omega_{sc} - \mathbf{k} \cdot \mathbf{V}, \tag{6}$$

where ω_{rest} is the rest frame frequency, $\omega_{sc} = 2\pi f_{sc}$ is the spacecraft frame frequency, and $\mathbf{V}$ the flow velocity. Figure 9 displays the 2-D cut of energy distribution in the $\omega_{sc} - k_z$ plane (Figure 9a) and the $\omega_{rest} - k_z$ plane (Figure 9b). While the energy distribution is determined in a rectangular window in the $\omega_{sc} - k_z$ plane, the window shape shifts to lower or negative frequencies at positive wave numbers (along the flow direction, k_z) and to even higher frequencies at negative wave numbers. The shape of coverage of the energy distribution resembles a parallelogram in the flow rest frame. Therefore the coverage of the energy distribution is not symmetrically spanned in the $\omega_{rest} - k_z$ plane. The missing area of the energy distribution in the rest frame (positive frequency regime at positive wave numbers, and negative frequency regime at negative wave numbers) results from the aliasing-free condition imposed previously.

[31] The next step is to apply the representation of absolute frequencies, that is the signs of frequency and wave vector are reversed if the wave component has a negative frequency in the rest frame:

$$(\omega_{rest}, \mathbf{k}) \rightarrow \begin{cases} (\omega_{rest}, \mathbf{k}) & \text{for} \quad \omega_{rest} \geq 0 \\ (-\omega_{rest}, -\mathbf{k}) & \text{for} \quad \omega_{rest} < 0 \end{cases} \tag{7}$$

For waves with positive frequencies no sign reversal is needed. The absolute frequency representation is convenient for projection of the 4-D energy distribution into the six planes because wave vector directions are the same as wave propagation directions. The negative frequency regime in Figure 9b (third quadrant) is reflected to the first quadrant in the absolute frequency representation. The cut of energy distribution in the $\omega_{rest} - k_z$ plane under this representation is displayed in Figure 9c. Most of fluctuation energy is identified at low frequencies below 0.5 rad/s. The coverage of the distribution is still asymmetric between the flow direction ($k_z > 0$) and its opposite direction ($k_z < 0$). Our measurement has a better coverage in the antiparallel direction to flow. This asymmetry is more pronounced as we move to higher frequencies. This result gives an experimental proof of the asymmetric coverage in the frequency and wave number domain discussed by *Sahraoui et al.* [2010].

[32] The main shortcoming of the asymmetry discussed here is that to obtain the 3-D k-spectra by integrating over ω_{rest} one is confined to the region of (ω_{rest}, $\mathbf{k}$), where the symmetry ($-\mathbf{k}$, $\mathbf{k}$) is guaranteed. From Figure 9c one can see that this region exists in the very low-frequency part of the spectrum. Fortunately, this region contains most of the energy. Figure 9 suggests the necessity of limiting the analysis to the symmetric domain defined by $\omega_{rest} < 0.20$ rad/s and $k < 0.0015$ rad/km. We note that this limit for ω_{rest} agrees with the Taylor frozen-in flow assumption. Indeed, if we consider the uncertainty in estimating the flow speed from the CIS data $\delta V_f \sim 20$ km/s, the resulting error in estimation of the Doppler shift ($\omega_{sc} \simeq \mathbf{k} \cdot \mathbf{V}$) is $\delta\omega_{sc} \simeq k\delta V_f \simeq 0.3$ rad/s, which essentially includes the band [0, ω_{rest}] = [0, 0.2] rad/s considered above.

4.3. Four-Dimensional Distribution in the Flow Rest Frame

[33] Figure 10 displays as our final results the 4-D energy distribution in the flow rest frame (absolute frequencies). Figure 10a does not show any particular dispersion pattern (recall that the mean magnetic field is almost aligned with the x-axis). To within uncertainties, this is consistent with solar wind turbulence being strong at these scales or frequencies (i.e., no linear dispersion relation is expected to be observed). Note, however, that under the present plasma conditions where the Alfvén speed about $V_A = 21$ km/s, the linear dispersion of that mode $\omega_{rest} = k_{\|}V_A$ cannot be resolved since it is at best of the order of the error in the estimation of the Doppler shift given above (it is even smaller if $k_{\|} \ll k_{\perp}$). The distribution exhibits an almost vertically extended structure in the $\omega_{rest} - k_z$ plane (in the flow direction) toward (ω_{rest}, k_z) = (0.20 rad/s, −0.0005 rad/km). Its apparent phase speed is about 400 km/s against the flow, suggesting that it originates most probably in the residual components at zero frequencies in the spacecraft frame. We interpret this slightly tilted, vertical structure in the energy distribution as representing a measurement effect rather than a phenomenon

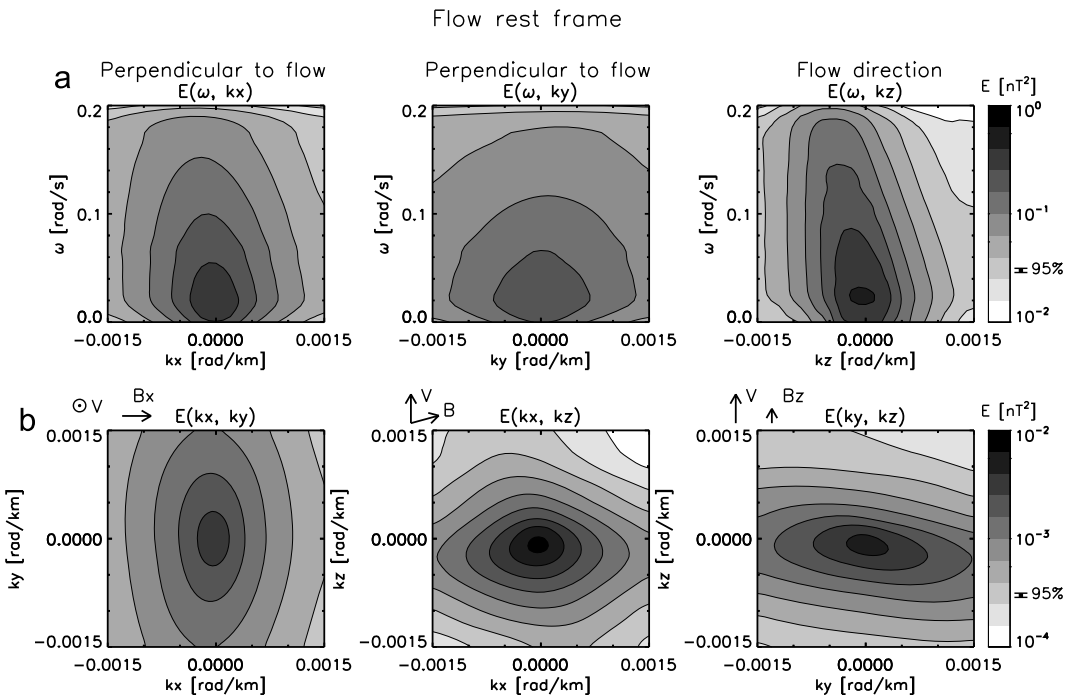

Figure 10. Energy distribution in the flow rest frame determined from Cluster solar wind data obtained on 12 March 2005. The same projection is used as Figure 1.

with a physically relevant origin. It is also interesting to note that the distribution is almost symmetric with respect to the sign of wave vectors, particularly in the $\omega_{rest} - k_x$ and $\omega_{rest} - k_y$ planes.

[34] Summing over the angular frequencies and averaging over a given wave vector component yields the reduced 2-D distributions shown in Figure 10b. The $k_x - k_y$ plane is perpendicular to the flow direction and the projected distribution exhibits an extended structure in the k_y direction, which is almost perpendicular to the mean magnetic field. The energy is minimum (or its decrease is largest) in the k_x direction, which is almost parallel to the mean magnetic field. The distribution is anisotropic with respect to the mean magnetic field but still is symmetric with respect to the signs of k_x and k_y. In the $k_x - k_z$ plane the distribution exhibits two extended directions. One is in the k_x direction where fluctuation energy is largest. Another extended structure is identified almost in the k_z direction (in the flow direction) but the extension is moderate. The distribution has the shape of cross in this plane and is extended to the x and the z axes (with a slight oblique angle from the z axis). The energy distribution is qualitatively symmetric with respect to the signs of k_x and k_z (the slight asymmetry with respect to the sign of k_z is a residual effect of the integration procedure described above, since the width of integrated frequencies $[0, \omega_{rest}] = [0, 0.2]$ rad/s has been only roughly estimated). In the k_y and k_z plane the distribution has an extended structure in the k_y direction (perpendicular to both the flow and the mean magnetic field) and energy is smallest in the k_z direction. The distribution is symmetric to the sign of k_y and also roughly symmetric with the sign of k_z.

[35] The difference of energy between the maximum and the minimum directions in the three planes of the wave vector projection can be determined and compared with their mean values. That energy difference is 59.6% in the $k_x - k_y$ plane, 98.3% in the $k_x - k_z$ plane, and 157% in the $k_y - k_z$ plane. The statistical error (the 95% confidence interval) is again smaller than the contour scale in Figure 10b. Therefore the double anisotropy identified in the energy distribution in Figure 10 is physically significant.

[36] To summarize: (1) In the flow rest frame 4-D energy distribution exhibits anisotropy such that it is elongated or extended almost along the k_x, k_y, and k_z directions, suggesting that anisotropy is largest in the direction perpendicular to both the flow and the mean magnetic field. (2) The distribution is almost symmetric with respect to the signs of wave vectors. (3) No linear wave dispersion relation can be identified. (4) Energy is maximum at smallest wave numbers and decreases monotonously toward larger wave numbers.

5. Discussion

[37] Anisotropy imposed by the mean magnetic field has been studied and discussed in a number of papers [*Matthaeus et al.*, 1990; *Bieber et al.*, 1994, 1996; *Spangler*, 1999]. The reported anisotropies represent a 2-D-turbulence geometry (energy distribution extended in the perpendicular direction to the mean magnetic field) or a slab geometry (extended in the parallel direction). Our results indicate that the energy distribution is elongated in the perpendicular direction to the magnetic field, which supports the picture of the 2-D turbulence geometry. Around the mean magnetic field, however, the energy distribution is not axially symmetric but is elongated in the perpendicular direction to the flow direction. The origin of this anisotropy is not altogether clear. One possible interpretation is that the mean flow direction itself has an effect in solar wind turbulence. For example, velocity shear may be present on a large spatial

scale that cannot be resolved by the Cluster spacecraft. This interpretation also prefers the picture that turbulence in the solar wind is actively pumped and driven by the large-scale velocity shear at the Earth's orbit, as suggested by *Roberts et al.* [1987a, 1987b]. In other words, the solar wind may not represent freely decaying turbulence. Another interpretation is motivated by a nongyrotropic spectrum observed in the magnetosheath turbulence [*Sahraoui et al.*, 2006]. That effect has been explained as being due to proximity to the magnetopause; the normal to the magnetopause acted as a boundary in one direction perpendicular to the mean magnetic field (and to the flow direction). Similar behavior due to the normal to the shock has been reported by *Yordanova et al.* [2008]. In the present case, we have compared the direction of extension of the energy distribution to the normal to the bow shock surface closest to the Cluster position using the model provided by *Farris and Russell* [1994], *Cairns et al.* [1995], and *Merka et al.* [2003]. The shock normal vector $\mathbf{n} = (-0.214, 0.321, -0.923)$ in the flow coordinate system is found to form a small angle with the flow direction (about 23°). This proximity to the bow shock may explain this second anisotropy in the plane perpendicular to the mean magnetic field. In other words, the shock normal may act as a constraint (or a boundary) that influences the turbulence to be stratified in planes perpendicular to it, as seen in magnetosheath turbulence [*Sahraoui et al.*, 2006; *Yordanova et al.*, 2008], although the solar wind is a supersonic and super-Alfvénic flow. It is also worthwhile to note that the estimated shock normal direction and the flow direction are nearly colinear (within uncertainties in their estimation), while in the case of magnetosheath they were quasi-perpendicular [*Sahraoui et al.*, 2006].

[38] Though we initially define a symmetric frequency and wave number domain, we have shown that the Doppler effect correction introduces asymmetry in the flow rest frame when combined with the limits for avoiding the aliasing effect, confirming the argument of *Sahraoui et al.* [2010]. The spectra are found to be more asymmetric (i.e., truncated) over the k_z axis as we move toward high frequencies in the flow rest frame. This is a fundamental limitation of measuring full wave number spectra for high-frequency phenomena. However, for low-frequency turbulence governed by the Taylor frozen-in flow approximation, it is possible to obtain the 3-D wave number spectra of turbulence and investigate anisotropic structure of the energy distribution. By limiting the energy distribution to the band of frequencies [0, 0.2] rad/km we have shown that the overall distribution is symmetric with respect to the sign of the wave vector. The slight residual asymmetry may be explained by the inaccuracy in estimation the Doppler shift. In this respect we recall that our analysis performs a Doppler correction using the bulk flow velocity measured by the CIS-HIA instrument. One could use electron data for the velocity measurements as the magnetic field is frozen in the electron fluid rather than the ion fluid if the Hall term in the generalized Ohm's law is taken into account. But at the analyzed wave numbers (spatial scale much larger than ion gyroradius) the Hall effect would not be significant.

[39] The absence of a dispersion relation in the energy distribution is consistent with the picture that the solar wind is in a well-developed turbulent state. The transition from linear modes to turbulence can in principle be understood as a change of dispersion relation, as it is not only a function of the wave number but also depends on the wave amplitude for large-amplitude waves [*Treumann and Baumjohann*, 1997]. A nonlinear dispersion relation is generally dependent on fluctuation amplitudes and therefore with large amplitude fluctuations the dispersion relation is not well defined and various combinations of frequencies and wave vectors are allowed to exist. Using direct numerical simulations, *Dmitruk and Matthaeus* [2009] also found that linear modes were only weakly present and that most of the power in the turbulence could not be associated with linear Alfvén modes. A more complete investigation of this question may require finding intervals with low Alfvén and sonic Mach numbers so that the frequency domain available for analysis is larger.

[40] Besides the spectra of turbulence studied here, higher-order statistics are needed to investigate other properties of the turbulence such as the wave-wave interactions and the resulting phase coherence and intermittency [*Sahraoui*, 2008]. The wave telescope technique can be further generalized to higher-order statistics [*Narita et al.*, 2008]. Combined analyses of energy distribution and higher-order statistics would advance our understanding of solar wind turbulence, for example, about the question of how the strength of mode coupling affects a power spectrum.

6. Conclusions

[41] We have demonstrated that the Cluster spacecraft can be used to determine the 4-D energy distribution in the flow rest frame. The 4-D energy distribution visualizes the spatiotemporal structure or the frequency-wave vector structure of magnetic field fluctuations in the solar wind. The major result is the identification of double anisotropy in the wave vector domain: One direction is associated with the mean magnetic field and the other with the flow direction or the shock normal direction. Energy is maximum perpendicular to the magnetic field as well as in the direction of the flow or the shock normal. This result is consistent with the picture of 2-D turbulence geometry imposed by the mean magnetic field. A more general analysis using more data intervals is needed to make definitive conclusions as to whether or not Alfvénic linear dispersion is present.

[42] **Acknowledgments.** The work of YN and KHG was financially supported by Bundesministerium für Wirtschaft und Technologie and Deutsches Zentrum für Luft- und Raumfahrt, Germany, under contract 50 OC 0901. FS is partly funded by the NPP program at NASA/GSFC. Discussion with S. P. Gary is greatly appreciated. We thank H. Rème and I. Dandouras for providing the ion data of Cluster.

[43] Wolfgang Baumjohann thanks Joachim Vogt and S. Gary for their assistance in evaluating this paper.

References

Balogh, A., et al. (2001), The Cluster magnetic field investigation: overview of in-flight performance and initial results, *Ann. Geophys.*, *19*, 1207–1217.

Bieber, J. W., W. H. Matthaeus, C. W. Smith, W. Wanner, M. -B. Kallenrode, and G. Wibberenz (1994), Proton and electron mean free paths: The Palmer consensus revisited, *Astrophys. J.*, *420*, 294–306.

Bieber, J. W., W. Wannger, and W. H. Matthaeus (1996), Dominant two-dimensional solar wind turbulence with implications for cosmic ray transport, *J. Geophys. Res.*, *101*, 2511–2522.

Biskamp, D. (2003), *Magnetohydrodynamic Turbulence*, 262 pp., Cambridge Univ. Press, Cambridge, U. K.

Cairns, I. H., D. H. Fairfield, R. R. Anderson, V. E. H. Carlton, K. I. Paularena, and A. J. Lazarus (1995), Unusual location of Earth's bow shock on September 24–25, 1987: Mach number effects, *J. Geophys. Res.*, *100*, 47–62.

Coleman, P. J., Jr. (1968), Turbulence, viscosity, and dissipation in the solar-wind plasma, *J. Geophys. Res.*, *153*, 371–388.

Dasso, S., L. J. Milano, W. H. Matthaeus, and C. W. Smith (2005), Anisotropy in fast and slow solar wind fluctuations, *Astrophys. J.*, *635*, L181–L184.

Dmitruk, P., and W. H. Matthaeus (2009), Waves and turbulence in magnetohydrodynamic direct numerical simulations, *Phys. Plasmas*, *16*, 062304.

Escoubet, C. P., M. Fehringer, and M. Goldstein (2001), The Cluster mission, *Ann. Geophys.*, *19*, 1197–1200.

Farris, M. H., and C. T. Russell (1994), Determining the standoff distance of the bow shock: Mach number dependence and use of models, *J. Geophys. Res.*, *99*, 17,681–17,689.

Glassmeier, K.-H., et al. (2001), Cluster as a wave telescope - First results from the fluxgate magnetometer, *Ann. Geophys.*, *19*, 1439–1447.

Horbury, T. S., and K. T. Osman (2008), Multi-spacecraft turbulence analysis methods, in *Multi-Spacecraft Analysis Methods Revisited*, *Sci. Rep. 8*, edited by G. Paschmann and P. W. Daly, pp. 55–64, Int. Space Sci. Inst., Bern.

Jenkins, G. M., and D. G. Watts (1968), *Spectral Analysis and its Applications*, pp. 313–317, Holden-Day, San Francisco.

Kolmogorov, A. N. (1941), The local structure of turbulence in incompressible viscous fluid for very large Reynolds' numbers, *Dokl. Akad. Nauk SSSR*, *30*, 301–305 (reprinted in *Proc. R. Soc. London Ser. A*, *434*, 9–13, 1991).

Leamon, R. J., C. W. Smith, N. F. Ness, W. H. Matthaeus, and H. K. Wong (1998), Observational constraints on the dynamics of the interplanetary magnetic field dissipation range, *J. Geophys. Res.*, *103*, 4775.

Marsch, E., and C.-Y. Tu (1990), On the radial evolution of MHD turbulence in the inner heliosphere, *J. Geophys. Res.*, *95*, 8211–8229.

Matthaeus, W. H., and M. L. Goldstein (1982), Measurement of the rugged invariants of magnetohydrodynamic turbulence in the solar wind *J. Geophys. Res.*, *87*, 6011–6028.

Matthaeus, W. H., M. L. Goldstein, and C. Smith (1982), Evaluation of magnetic helicity in homogeneous turbulence, *Phys. Rev. Lett.*, *48*, 1256–1259.

Matthaeus, W. H., M. L. Goldstein, and D. A. Roberts (1990), Evidence for the presence of quasi-two-dimensional nearly incompressible fluctuations in the solar wind, *J. Geophys. Res.*, *95*, 20,673–20,683.

Merka, J., A. Szabo, T. W. Narock, J. H. King, K. I. Paularena, and J. D. Richardson (2003), A comparison of IMP 8 observed bow shock positions with model predictions, *J. Geophys. Res.*, *108*(A2), 1077, doi:10.1029/2002JA009384.

Motschmann, U., T. I. Woodward, K. H. Glassmeier, D. J. Southwood, and J. L. Pinçon (1996), Wavelength and direction filtering by magnetic measurements at satellite arrays: Generalized minimum variance analysis, *J. Geophys. Res.*, *101*, 4961–4966.

Narita, Y., and K.-H. Glassmeier (2005), Dispersion analysis of low-frequency waves through the terrestrial bow shock, *J. Geophys. Res.*, *110*, A12215, doi:10.1029/2005JA011256.

Narita, Y., and K.-H. Glassmeier (2006), Propagation pattern of low frequency waves in the terrestrial magnetosheath, *Ann. Geophys.*, *24*, 2441–2444.

Narita, Y., and K.-H. Glassmeier (2009), Spatial aliasing and distortion of energy distribution in the wave vector domain under multi-spacecraft measurements, *Ann. Geophys*, *27*, 3031–3042.

Narita, Y., K.-H. Glassmeier, S. Schäfer, U. Motschmann, K. Sauer, I. Dandouras, K.-H. Fornaçon, E. Georgescu, and H. Rème (2003), Dispersion analysis of ULF waves in the foreshock using cluster data and the wave telescope technique, *Geophys. Res. Lett.*, *30*(13), 1710, doi:10.1029/2003GL017432.

Narita, Y., et al. (2004), Alfvén waves in the foreshock propagating upstream in the plasma rest frame: Statistics from Cluster observations, *Ann. Geophys.*, *22*, 2315–2323.

Narita, Y., K.-H. Glassmeier, K.-H. Fornaçon, I. Richter, S. Schäfer, U. Motschmann, I. Dandouras, H. Rème, and E. Georgescu (2006a), Low-frequency wave characteristics in the upstream and downstream regime of the terrestrial bow shock, *J. Geophys. Res.*, *111*, A01203, doi:10.1029/2005JA011231.

Narita, Y., K.-H. Glassmeier, and R. A. Treumann (2006b), Wave-number spectra and intermittency in the terrestrial foreshock region, *Phys. Rev. Lett.*, *97*, 191101, doi:10.1103/PhysRevLett.97.191101.

Narita, Y., K.-H. Glassmeier, M. Fränz, Y. Nariyuki, and T. Hada (2007), Observations of linear and nonlinear processes in the foreshock wave evolution, *Nonlinear Proc. Geophys.*, *14*, 361–371.

Narita, Y., K.-H. Glassmeier, P. M. E. Décréau, T. Hada, U. Motschmann, and Y. Nariyuki (2008), Evaluation of bispectrum in the wave number domain based on multi-point measurements, *Ann. Geophys.*, *26*, 3389–3393.

Neubauer, F. M., and K.-H. Glassmeier (1990), Use of an array of satellites as a wave telescope, *J. Geophys. Res.*, *95*, 19,115–122.

Pinçon, J. L., and F. Lefeuvre (1988), Characterization of a homogeneous field turbulence from multipoint measurements, *Adv. Space Res.*, *8*, 459–462.

Pinçon, J. L., and F. Lefeuvre (1991), Local characterization of homogeneous turbulence in a space plasma from simultaneous measurements of field components at several points in space, *J. Geophys. Res.*, *96*, 1789–1802.

Pinçon, J. L., and U. Motschmann (1998), Multi-spacecraft filtering: General framework, in *Analysis Methods for Multi-Spacecraft Data*, edited by G. Paschmann and P. W. Daly, pp. 65–90, Int. Space Sci. Inst., Bern.

Podesta, J. J., D. A. Roberts, and M. L. Goldstein (2007), Spectral exponents of kinetic and magnetic energy spectra in solar wind turbulence, *Astrophys. J.*, *664*, 543–548, doi:10.1086/519211.

Robert, P., A. Roux, C. C. Harvey, M. W. Dunlop, P. W. Daly, and K.-H. Glassmeier (1998), Tetrahedron geometric factors, in *Analysis Methods for Multi-Spacecraft Data*, *Sci. Rep. SR-001*, edited by G. Paschmann and P. W. Daly, pp. 323–348, Int. Space Sci. Inst., Bern.

Roberts, D. A., M. L. Goldstein, L. W. Klein, and W. H. Matthaeus (1987a), Origin and evolution of fluctuations in the solar wind: Helios observations and Helios-Voyager comparison, *J. Geophys. Res.*, *92*, 12,023–12,035.

Roberts, D. A., L. W. Klein, M. L. Goldstein, and W. H. Matthaeus (1987b), The nature and evolution of magnetohydrodynamic fluctuation in the solar wind: Voyager observations, *J. Geophys. Res.*, *92*, 11,021–11,040.

Rème, H., et al. (2001), First multispacecraft ion measurements in and near the Earth's magnetosphere with the identical Cluster ion spectrometry (CIS) experiment, *Ann. Geophys.*, *19*, 1303–1354.

Sahraoui, F. (2008), Diagnosis of magnetic structures and intermittency in space-plasma turbulence using the technique of surrogate data, *Phys. Rev. E*, *78*, 026402.

Sahraoui, F., et al. (2003), ULF wave identification in the magnetosheath: The k-filtering technique applied to Cluster II data, *J. Geophys. Res.*, *108*(A9), 1335, doi:10.1029/2002JA009587. (Correction, *109*, A04222, doi10.1029/2004JA010469, 2004).

Sahraoui, F., G. Belmont, J. L. Pinon, L. Rezeau, A. Balogh, P. Robert, and N. Cornilleau-Wehrlin (2004), Magnetic turbulent spectra in the magnetosheath: New insights, *Ann. Geophys.*, *22*, 2283–2288.

Sahraoui, F., G. Belmont, L. Rezeau, N. Cornilleau-Wehrlin, J. L. Pinon, and A. Balogh (2006), Anisotropic turbulent spectra in the terrestrial magnetosheath as seen by the Cluster spacecraft, *Phys. Rev. Lett.*, *96*, 075002, doi:10.1103/PhysRevLett.96.075002.

Sahraoui, F., G. Belmont, M. L. Goldstein, and L. Rezeau (2010), Limitations of multispacecraft data techniques in measuring wavenumber spectra of space plasma turbulence, *J. Geophys. Res.*, doi:10.1029/2009JA014724, in press.

Spangler, S. R. (1999), Two-dimensional magnetohydrodynamics and interstellar plasma turbulence, *Astrophys. J.*, *522*, 879–896.

Taylor, G. I. (1938), The spectrum of turbulence, *Proc. R. Soc. London, Ser. A*, *164*, 476–490.

Treumann, R., and W. Baumjohann (1997), *Advanced Space Plasma Physics*, 287 pp., Imperial Coll. Press, London.

Tjulin, A., J. L. Pinçon, F. Sahraoui, M. André, and N. Cornilleau-Wehrlin (2005), The k-filtering technique applied to wave electric and magnetic field measurements from the Cluster satellites, *J. Geophys. Res.*, *110*, A11224, doi:10.1029/2005JA011125.

Vogt, J., Y. Narita, and O. D. Constantinescu (2008), The wave surveyor technique for fast plasma wave detection in multi-spacecraft data, *Ann. Geophys.*, *26*, 1699–1710.

Yordanova, E., A. Vaivads, M. André, S. C. Buchert, and Z. Vörös (2008), Magnetosheath plasma turbulence and its spatiotemporal evolution as observed by the Cluster spacecraft, *Phys. Rev. Lett.*, *100*, 205003.

K.-H. Glassmeier and Y. Narita, Institut für Geophysik und extraterrestrische Physik, Technische Universität Braunschweig, Mendelssohnstr. 3, D-38106 Braunschweig, Germany. (y.narita@tu-bs.de)

M. L. Goldstein and F. Sahraoui, Geospace Physics Laboratory, NASA Goddard Space Flight Center, Code 673, Greenbelt, MD 20771, USA.